Ductile Cu–Al–Mn based shape memory alloys: general properties and applications

Y. Sutou[1], T. Omori[1], R. Kainuma*[2] and K. Ishida[1]

Polycrystalline Cu–Al–Mn shape memory alloys (SMAs) with a low degree of order of the β ($L2_1$) phase show excellent ductility and exhibit shape memory (SM) properties such as superelasticity, the one way memory effect and the two way memory effect based on martensitic transformation. These SM properties can be greatly enhanced by controlling microstructural factors such as grain size and texture by thermomechanical treatments. In the present paper, the SM properties of ductile Cu–Al–Mn based SMAs and microstructure control to obtain excellent SM characteristics are reviewed. Furthermore, an example of the application of Cu–Al–Mn based SMAs to a guidewire for medical use is also presented.

Keywords: Shape memory alloys, Medical devices, Microstructure control, Superelasticity

Introduction

Shape memory alloys (SMAs) such as Ni–Ti based, Cu based and Fe–Mn–Si based alloys have commercial potential for practical applications of SM properties and are drawing attention as high damping materials. Among these SMAs, Cu based SMAs are the most attractive for practical applications because of their low cost and relatively good SM properties. However, the highly ordered Cu based SMAs such as Cu–Al–Ni and Cu–Zn–Al with a polycrystalline structure are too brittle to be sufficiently cold worked. Many attempts to improve the ductility of these Cu based SMAs by grain refining have been made, but only limited success has been reported.[1,2]

In 1995, Kainuma *et al.*[3,4] first reported that Cu–Al–Mn alloys with low Al composition <17 at.-% show an excellent ductility and that polycrystalline alloys have potential for use as practical SMAs. So far, many kinds of properties such as one way memory effect (OWME),[4,5] two way memory effect (TWME),[6] superelasticity (SE),[4,7–9] dumping property (DP)[10] and low thermal expansion[11,12] in Cu–Al–Mn based SMAs have been investigated and microstructural control of such factors as grain size[7,8] and texture[9] controls have been shown to drastically improve the SE properties to the level of NiTi alloys. Recently, some attempts to apply this alloy system to practical use have begun.[12]

In the present paper, recent progress on Cu–Al–Mn based SMAs with prominent SM characteristics is presented and application to a guidewire for medical use is introduced as one example.

[1]Department of Materials Science, Graduate School of Engineering, Tohoku University, Aoba yama 6-6-02, Sendai 980 8579, Japan
[2]Institute of Multidisciplinary Research for Advanced Materials (IMRAM), Tohoku University, Katahira 2-1-1, Sendai 980 8577, Japan

*Corresponding author, email kainuma@tagen.tohoku.ac.jp

Alloy design for ductile SMA

Ductility and shape memory effect

Figure 1*a* and *b* shows an isothermal section diagram at 800°C and a vertical section diagram of the Cu–Al–10 at.-%Mn section respectively.[13] It can be seen that the single phase β region is broadened by the addition of Mn and that the transition temperatures associated with two types of order–disorder transitions, A2 to B2 and B2 to $L2_1$, in the β phase region drastically decrease with decreasing Al content. This vertical diagram in Fig. 1*b* suggests that the degree of order in the β parent phase may decrease with decreasing Al content. Actually, in the high Al composition range >16 at.-%Al, the ordering to the $L2_1$ structure cannot be suppressed by quenching from the disordered A2 phase region, and the $L2_1$ phase martensitically transforms into a 6M structure with six layered modulation. However, in the low Al composition range <16 at.-%, the ordering from the A2 to the $L2_1$ structure can be suppressed by quenching and the martensitic transformation from the A2 to the 2M (disordered fcc) structure occurs at low temperature.[4] Figure 2 shows the dependence of Al content on cold workability, tensile elongation and shape recovery.[3,4] Here, the cold workability was evaluated using the cold workability parameter W which was defined as $W=(t_0-t_{min})/t_0\times100$, where t_0 and t_{min} are the initial thickness and the minimum thickness before a crack appeared during cold rolling at room temperature respectively. It is seen that the ductility and elongation drastically increase with decreasing Al content, and that in the composition range <17 at.-%Al, the cold workability > 60% and tensile elongation >10% can be obtained because of a low degree of order in the parent phase. Figure 2 also shows the dependence of Al content on the shape recovery estimated by a simple bending test.[5] It is seen that the $L2_1$ alloys with a low degree of order show good shape recovery, although such recovery

Published by Maney on behalf of the Institute
Received 24 August 2007; accepted 29 October 2007
DOI 10.1179/174328408X302567

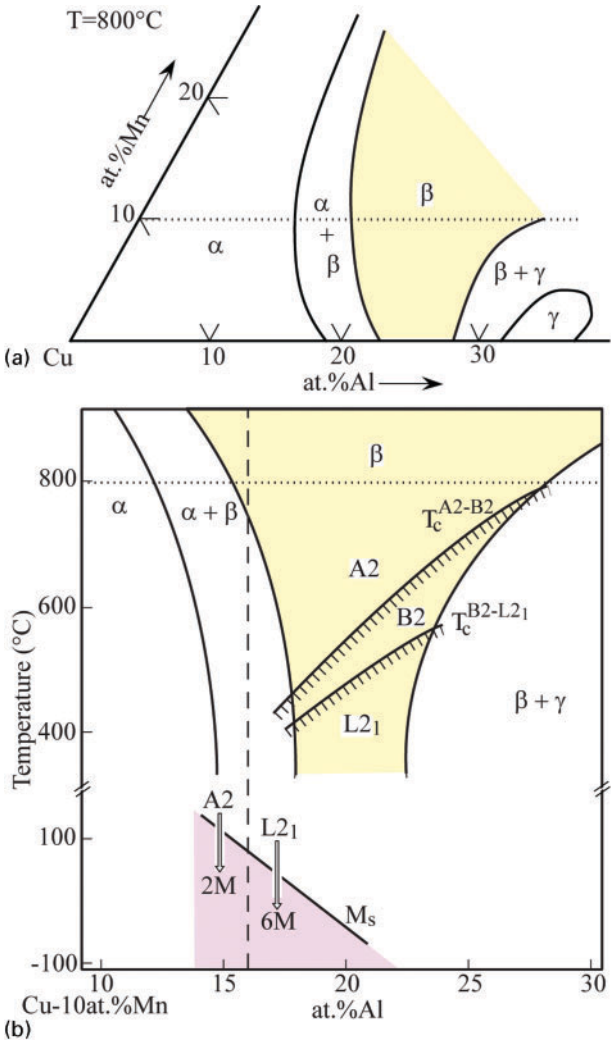

1 ***a*** **isothermal section diagram at 800°C and** ***b*** **vertical section diagram in Cu–Al–10 at.-%Mn ternary system with A2/B2 (T_c^{A2-B2}) and B2/$L2_1$ (T_c^{B2-L21}) order–disorder transformation and martensitic transformation starting M_s temperatures[4,13]**

slightly decreases in the low Al alloys with the A2 parent phase.

From these results it can be summarised that the alloys with Al content between 16 and 18 at.-% may have a good balance between excellent workability and shape memory properties.

Transformation temperatures

Martensitic transformation temperatures of ternary Cu–Al–Mn alloys have been investigated by various researchers.[14–17] According to the previous results, the martensitic starting temperature M_s in the high Al composition region >20 at.-% can be expressed as a linear relation. However, as shown in Fig. 3*a*, in the low Al composition range <20 at.-%, the composition dependence of the M_s cannot be described by the above equation in a linear relation.[3,4] The deviation from straight iso-M_s lines is attributed to the change in the degree of order in the parent β phase. This is confirmed by a fact that the M_s temperature of as quenched specimens drastically increases by low temperature aging, which induces the increase of the degree of order as shown in Fig. 3*b*.[3,4] Since the ordering reaction

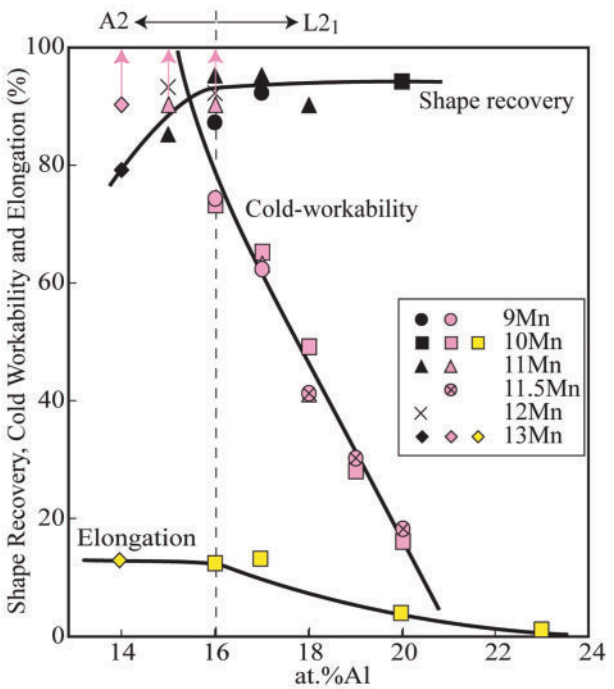

2 Effect of Al content on cold workability, tensile elongation and shape recovery obtained by bending test in Cu–Al–(9–13) at.-%Mn alloys with β single phase[3,5]

proceeds and the M_s gradually increase with time even at room temperatures, stabilisation treatment due to low temperature aging at 150–200°C is required before practical use of these alloys.

Effects of alloying elements such as Ti, Cr, Fe, Co, Ni, Ag, Au, Zn, Si and Sn on the M_s temperature in $Cu_{73}Al_{17}Mn_{10}$ alloy have been previously reported.[5]

Superelasticity

Improvement of SE due to grain size control

It is known that SM properties depend on the grain size of the parent phase.[18,19] Recently, it has been found that recoverable strain increases with increasing relative grain size for sheet or wire specimens, which is defined by the relation d/t or d/D, where d, t and D are the mean grain diameter, the thickness of sheet and the diameter of wire specimen respectively.[7,8]

Figure 4 shows the stress–strain curves obtained by tensile cyclic testing of wire specimens with different d/D.[8] The cyclic testing was carried out at A_f+30°C at a strain rate of 0·5 mm min^{-1} and a gauge length of tensile specimen of 50 mm; details of the experimental method employed in cyclic testing have been described in the authors' previous reports.[4,8] Some specimens with different d/D were prepared using various thermomechanical treatments and were finally solution treated at 800–950°C followed by aging at 200°C. As shown in the figures, the stress–strain characteristics are strongly dependent on the value of the d/D. With decreasing d/D, the yield stress σ_t and the work hardening rate after yielding $\delta\sigma_{SE}/\delta\varepsilon$ increase and the recovery strain decreases. Figure 5 shows the dependence of the applied strain ($\varepsilon_t{}^i-\varepsilon_e{}^i$) on the $\varepsilon_{SE}{}^i$ in the specimens indicated in Fig. 4, where $\varepsilon_t{}^i$ and $\varepsilon_e{}^i$ are the applied strain and the genuine elastic strain respectively.[8] The SE strain is defined as $\varepsilon_{SE}{}^i=\varepsilon_t{}^i-\varepsilon_e{}^i-\varepsilon_r{}^i$ in which $\varepsilon_r{}^i$ is the residual strain after removal of the stress and i is the

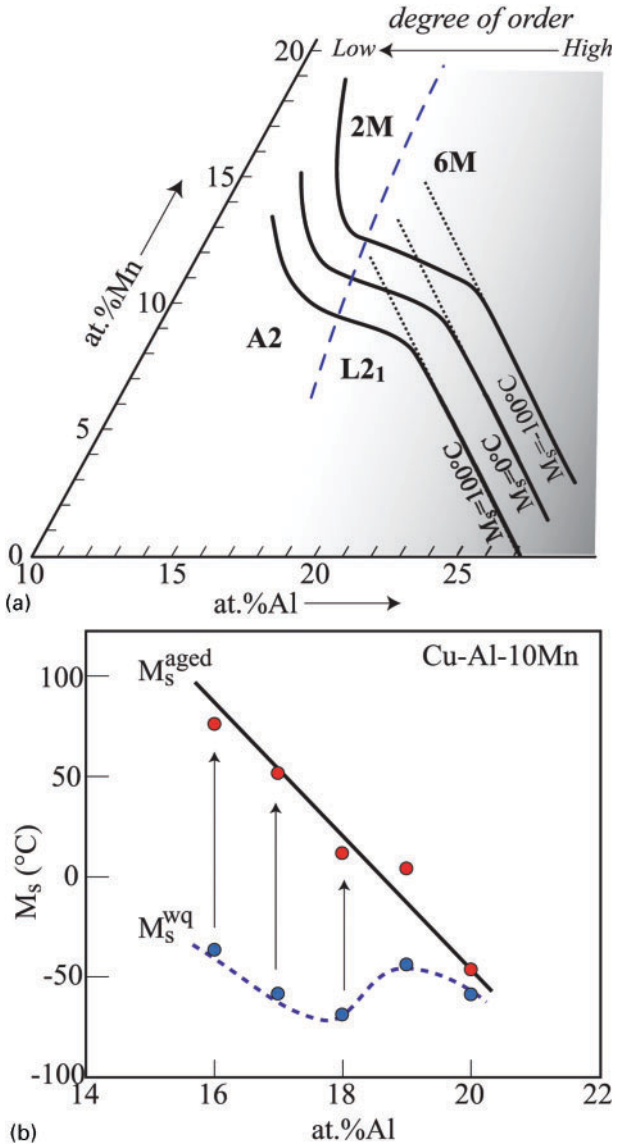

3 *a* contour of iso-M_s composition lines in β phase and *b* M_s temperatures of as quenched and as aged specimens[3]

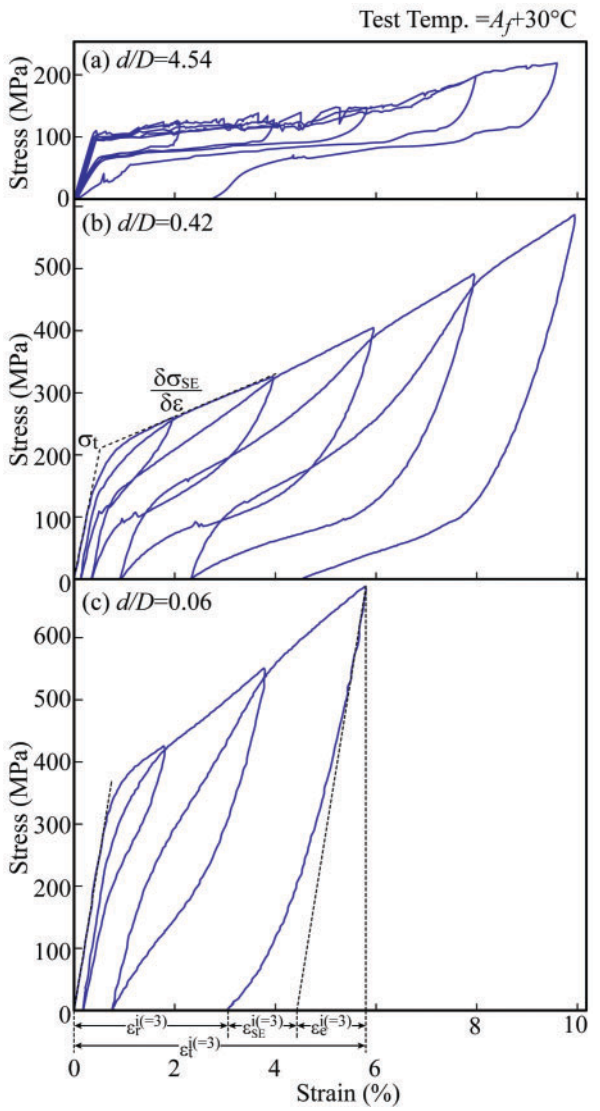

4 Cyclic stress–strain curves obtained from specimens with *d/D* values of *a* 4·54, *b* 0·42 and *c* 0·06 at temperature of A_f+30°C (Ref. 8)

number of cycles as illustrated in Fig. 4*c*. It can be seen that the $\varepsilon_{SE}{}^{i}$ increases with increasing $\varepsilon_t{}^{i}-\varepsilon_e{}^{i}$ in the initial stage and then decreases after reaching the maximum point, which is defined as the maximum SE strain $\varepsilon_{SE}{}^{MAX}$. It is noted that $\varepsilon_{SE}{}^{MAX}$ increases with increasing *d*/*D* and that a large SE strain of ~7%, which is nearly equal to that of Ni–Ti SMAs, can be obtained in the specimen with *d*/*D*=4·54, while that of the specimen with *d*/*D*=0·06 is <2%. The obtained σ_t and $\varepsilon_{SE}{}^{MAX}$ in the specimens with various *d*/*D* values are almost proportional to a function $[1-(d/D)]^2$ which is the area ratio of the grains perfectly surrounded by neighbouring grains in the cross-sectional area of the wire, as shown in Fig. 6.[8] Details on this analysis have been previously reported.[8]

Enhancement of SE due to texture control

The development of texture is one of the most effective methods for improving the SM properties, and the formation of a particular texture by means of the thermomechanical process (TMP),[20,21] rapid solidification,[22,23] sputtering,[24] and so on have been attempted. However, it is difficult to utilise the TMP techniques of

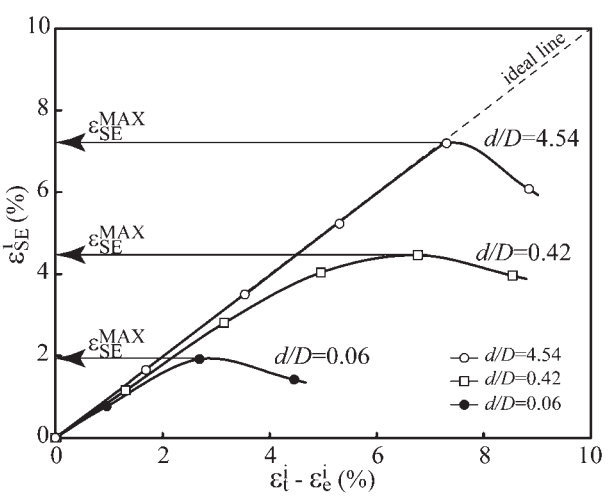

5 Plot of SE strain ε_{SE}^{i} versus applied strain $\varepsilon_t^i-\varepsilon_e^i$ in specimens with various *d/D* values[8]

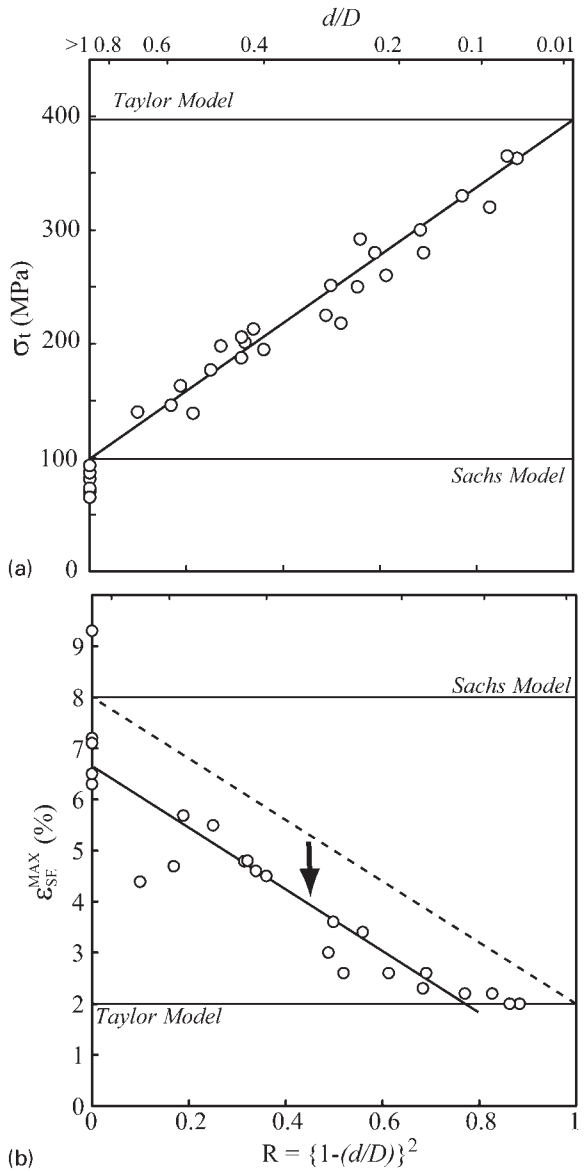

6 Plots of *a* critical stress σ_t and *b* SE maximum strain ε_{SE}^{MAX} against $[1-(d/D)]^2$ (Ref. 8)

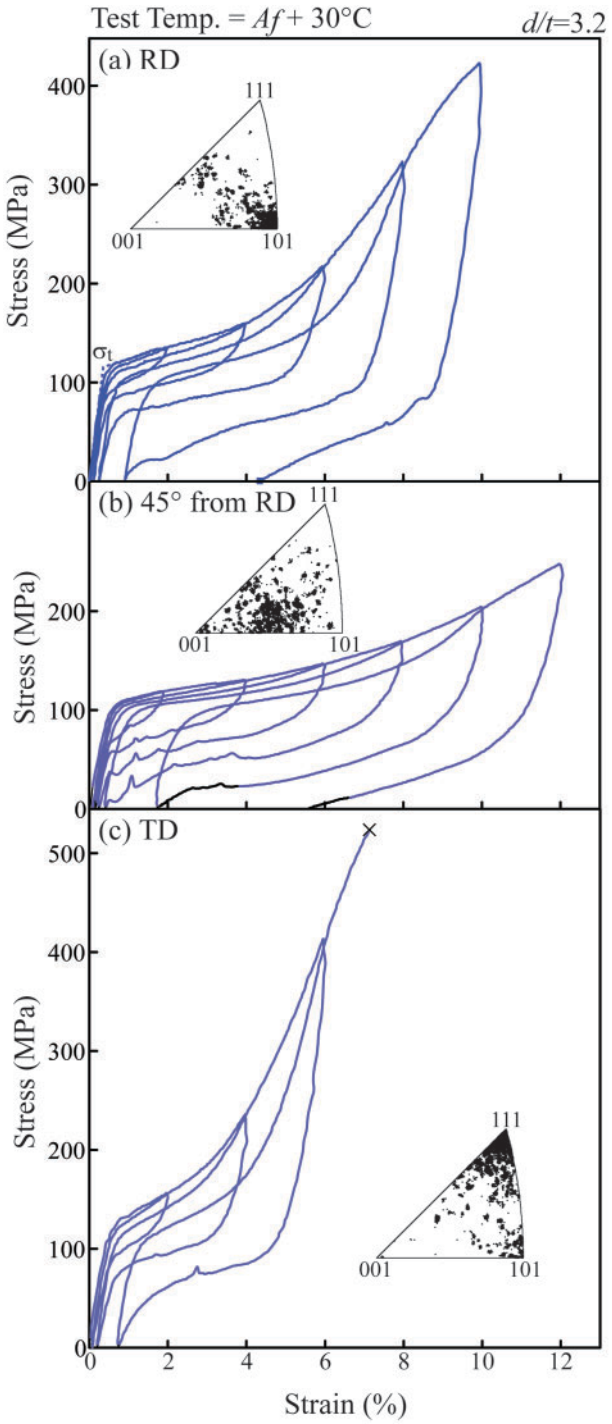

7 Cyclic stress–strain curves obtained from specimens cut along loading direction *a* RD, *b* 45° from RD and *c* TD in $(Cu_{73\cdot5}Al_{17}Mn_{9\cdot5})_{97}$–$Ni_3$ sheet plane, where cyclic testing was carried out at A_f+30°C (Ref. 9)

texture control for improving the SM properties of conventional Cu based SMAs such as Cu–Al–Ni and Cu–Zn–Al alloys because of their low cold workability. The authors have found that the TMP can be utilised for texture control of the ductile Cu–Al–Mn alloys and that a strong {112}<110> recrystallisation texture can be developed by the addition of Ni to Cu–Al–Mn ternary alloy and by using TMP treatment with heavy cold rolling.[9]

The stress–strain characteristics of the above mentioned textured specimen aged at 200°C were investigated using tensile cyclic testing.[9] Figure 7 shows the stress–strain curves of specimens cut out in the rolling direction (RD), at an angle of 45° from the RD or 45° from the transverse direction (TD) and in the TD respectively, where these specimens have a relative grain size of $d/t=3\cdot2$. The stereotriangles in Fig. 7 show that the texture characteristics in each specimen and the texture densities in the RD, 45° and TD directions have their largest value around the [110], [102] and [111] directions respectively. It is also seen from Fig. 7 that the degree of SE is strongly dependent on the loading direction. Figure 8*a* shows the maximum SE strain ε_{SE}^{MAX} against the testing angle from the RD for textured $(Cu_{73\cdot5}Al_{17}Mn_{9\cdot5})_{97}$–$Ni_3$ sheet specimens, where the ε_{SE}^{MAX} is obtained in the same way as that of Fig. 4.[9] It is shown that the highest SE strain is obtained at ~45°, while the TD specimens exhibit the smallest value of the textured sheets. Figure 8*a* also shows the effect of d/t on the ε_{SE}^{MAX} in the textured sheets. The textured specimen with $d/t=3\cdot2$ exhibits a large SE strain of ~7·5% at a loading direction of 45° from RD, while the non-textured specimen with $d/t\approx3\cdot0$ shows an SE strain of ~5·5%. Figure 8*b* shows the orientation dependence of transformation strain in Cu–Al–Mn single crystal, which is

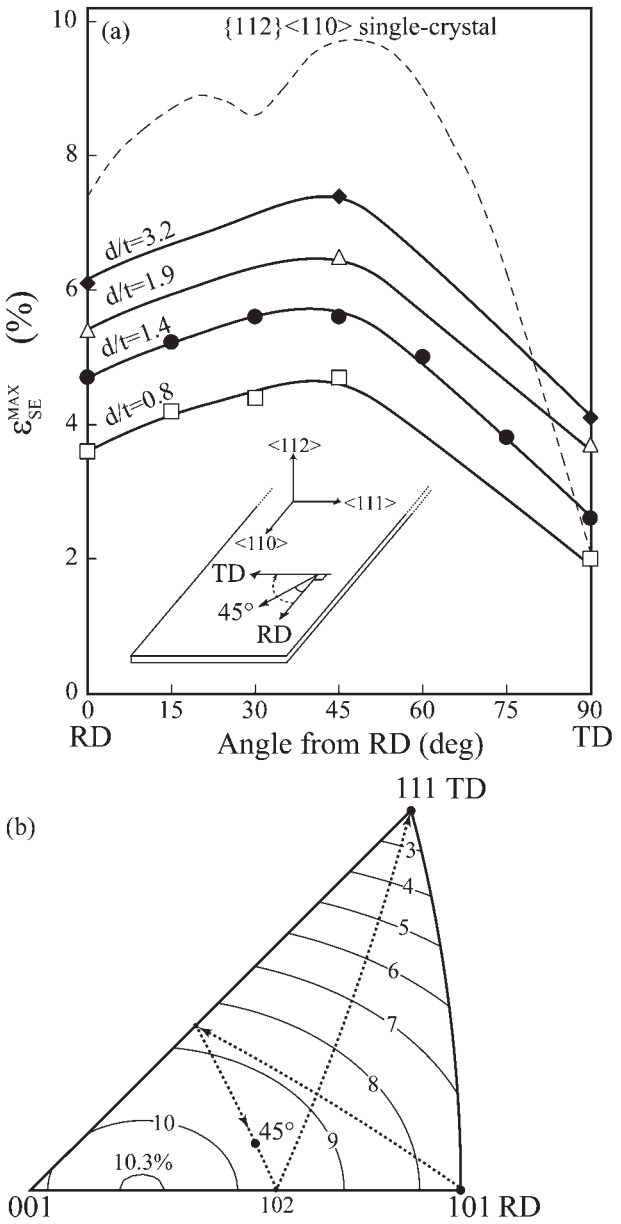

8 ***a*** **relationship between maximum SE strain ε_{SE}^{MAX} and angle from RD in {112}<110> textured $(Cu_{73{\cdot}5}Al_{17{\cdot}5}Mn_{9{\cdot}0})_{97}$–$Ni_3$ sheet with various *d/t* values (loading angle dependence on ε_{SE}^{MAX} in {112}<110> single crystal is also shown) and** ***b*** **counter lines of iso-transformation strain induced by $L2_1$/6M transformation obtained by calculation (rotation of loading direction in sheet plane from RD to TD as shown in inset in** ***a*** **corresponds to direction of path from RD to TD as indicated by broken line in** ***b*****)[9]**

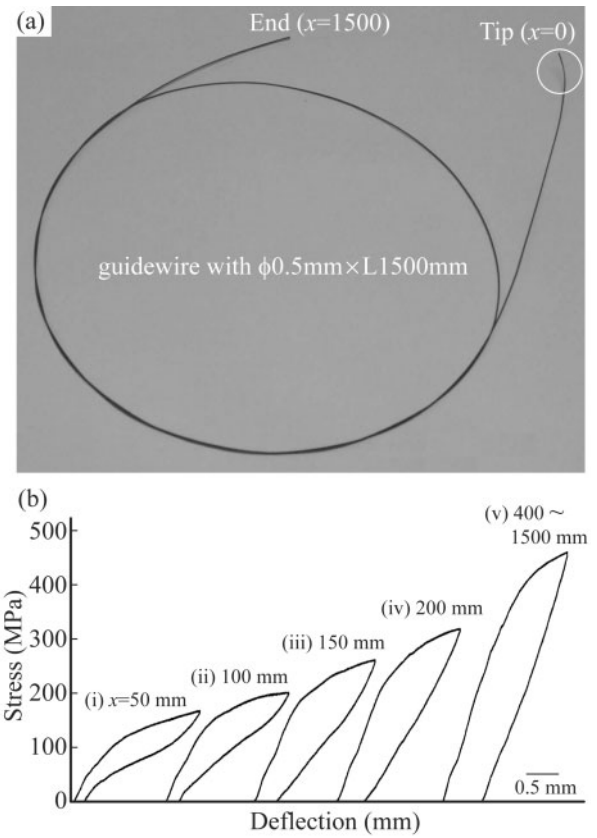

9 ***a*** **Cu–Al–Mn based guidewire with functionally graded properties and** ***b*** **stress deflection curves in each portion of Cu–Al–Mn based guidewire with graded microstructure, where solution treated wire was aged by using furnace with graded temperature, lowest and highest temperature being 200 and 325°C respectively[25]**

calculated on the basis of the phenomenological theory.[9] The direction path RD≥45°≥TD indicated by the broken line in Fig. 8*b* corresponds to the rotation path from RD to TD in the sheet plane with the {112}<110> texture as shown in inset in Fig. 8*a*, where the dependence of the testing angle on the transformation strain for the {112}<110> single crystal theoretically predicted from Fig. 8*b* is also shown. It can be seen that the anisotropy of the SE strain for the textured specimens has almost the same tendency as the prediction based on transformation strain for the single crystal.

Practical application of Cu–Al–Mn based SMAs

Since the Cu–Al–Mn based SMAs show excellent ductility and prominent SM characteristics as mentioned

Table 1 Shape memory characteristics for Cu–Al–Mn based, Ni–Ti, Cu–Zn–Al and Cu–Al–Ni SMA:6–29*

	Transformation Temp., °C	Cold workability, %	SE, %	OWME, %	TWME, %	DP§, (tanϕ)	Refs.
Cu–Al–Mn based	−200 to 150	>60	7·5	~10†	3·2(2·2) ‡	0·54	3–10
Ni–Ti	−40 to 100	~30	8	8	5	0·1	26–29
Cu–Zn–Al	−200 to 120	~30	2	5	2	0·12	26–29
Cu–Al–Ni	−200 to 170	~10	2	5	2	–	26–29

*SE is the superelasticity, OWME and TWME are the one and two way memory effects respectively and DP is the damping properties and is determined by dynamic mechanical spectroscopy.
†Surface strain obtained by bending test.
‡Surface strain induced by bending deformation, and value indicated in a parenthesis is TWME strain induced by tensile deformation.
§Peak value in tanϕ versus temperature curve obtained from measurement.

above, the application of these SMAs to various fields can be expected. Herein, the authors describe an example of the application of Cu–Al–Mn based SMAs to a guidewire for medical use.[25] Figure 9*a* shows a $\phi 0{\cdot}5$ mm $\times$ *L*1500 mm Cu–Al–Mn based guidewire coated with resin. The tip of the guidewire shows an excellent SE and is angled to improve its maneuverability in branched blood vessels as shown in Fig. 9*a*. In addition, this Cu–Al–Mn based guidewire possesses functionally graded characteristics which can be obtained by controlling the microstructure.[25] Figure 9*b* shows the dependence of the guidewire length *x* from the tip on the bending deflection curves obtained by a three point bending test at room temperature, where the centre of the bending test sample corresponds to the *x* position. Here, the gauge span for the three point bending test was 14 mm and a rough value of radius of curvature at the maximum deflection was $\sim$8 mm, in which the maximum surface strain applied on the wire is $\sim 3{\cdot}1\%$. It can be seen that the portion of guidewire from the tip to $x \approx 50$ mm shows excellent flexibility and SE, which can be obtained by relative grain size control, while the portion of the guidewire from $x \approx 400$ mm to the end shows high stiffness and strength and hardly exhibits the SE property. Furthermore, those properties are gradually varied in the range from $x \approx 50$ to 400 mm. Such enhancements of the stiffness and strength are caused by bainitic transformation induced by aging at around 200–400°C and the graded properties can be obtained by aging treatment using a furnace with a temperature gradient. Showing excellent pushability and torquability,[25] this wire with functionally graded properties is expected to be employed a new type of guidewire for catheterisation.

Conclusions

Cu–Al–Mn based SMAs have excellent ductility and show excellent SE, OWME, TWME, high damping characteristic and fatigue properties due to the addition of alloying elements, relative grain size and texture control. The maximum SM characteristics obtained in Cu–Al–Mn based SMAs are summarised in Table 1 compared with those in Ni–Ti, Cu–Zn–Al and Cu–Al–Ni SMAs.[26–29] The SM characteristics of the Cu–Al–Mn based SMAs are superior to those of the other Cu based SMAs and are almost equal to those of Ni–Ti SMAs. It can be concluded that the Cu–Al–Mn based SMAs have high potential for practical applications as SMAs in medical and electrical devices, micromachines, etc.

Acknowledgements

The authors are grateful to professor K. Yamauchi (Tohoku University) and professor T. Mori (the University of Manchester) for their helps in carrying out the application study and in preparation of the manuscript respectively. The present work was supported by Grant-in-Aids for Science Research from the Ministry of Education, Science, Sports and Culture, Japan.

Reference

1. S. Miyazaki and K. Otsuka: *Iron Steel Inst. Jpn Int.*, 1989, **29**, 353–377.
2. T. Tadaki: in 'Shape memory materials', (ed. K. Otsuka and C. M. Wayman), 97–116; 1998, Cambridge, Cambridge Univesity Press.
3. R. Kainuma, S. Takahashi and K. Ishida: *J. Phys. IV*, 1995, **5**, C8–961–966.
4. R. Kainuma, S. Takahashi and K. Ishida: *Metall. Mater. Trans. A*, 1996, **27A**, 2187–2195.
5. Y. Sutou, R. Kainuma and K. Ishida: *Mater. Sci. Eng. A*, 1999, **A275**, 375–379.
6. T. Omori, J. J. Wang, Y. Sutou, R. Kainuma and K .Ishida: *Mater. Trans.*, 2002, **43**, 1676–1683.
7. Y. Sutou, T. Omori, T. Okamoto, R. Kainuma and K. Ishida: *J. Phys. F. IV France*, 2001, **11**, 185–190.
8. Y. Sutou, T. Omori, K. Yamauchi, N. Ono, R. Kainuma and K. Ishida: *Acta Mater.*, 2005, **53**, 4121–4133.
9. Y. Sutou, T. Omori, R. Kainuma, N. Ono and K. Ishida: *Metall. Mater. Trans. A*, 2002, **33A**, 2817–2824.
10. N. Koeda, T. Omori, Y. Sutou, H. Suzuki, M. Wakita, R. Kainuma and K. Ishida: *Mater. Trans.*, 2005, **46**, 118–122.
11. R. Kainuma, J. J. Wang, T. Omori, Y. Sutou and K. Ishida: *Appl. Phys. Lett.*, 2002, **80**, 4348–4350.
12. Y. Sutou, T. Omori, J. J. Wang, R. Kainuma and K. Ishida: *Mater. Sci. Eng. A,* 2004, **A378**, 278–282.
13. R. Kainuma, N. Satoh, X. J. Liu, I. Ohnuma and K. Ishida: *J. Alloys Compd*, 1998, **266**, 191–200.
14. C. L. del Castillo, B. G. Mellor, M. L. Blazquez and C. Gomez: *Scr. Metall.*, 1987, **21**, 1711–1716.
15. S. J. L. Kang, M. Stasi and P. Azou: *Mem. Etud. Sci. Rev. Metall.*, 1982, **79**, 229–234.
16. K. Matsushita, T. Okamoto and T. Okamoto: *J. Mater. Sci.*, 1985, **20**, 689–699.
17. J. M. Guilemany and F. Peregrin: *J. Mater. Sci.*, 1992, **27**, 863–868.
18. I. Dvorak and E. B. Hawbolt: *Metall. Trans. A*, 1975, **6A**, 95–99.
19. G. N. Sure and L. C. Brown: *Metall. Trans. A.*, 1984, **15A**, 1613–1621.
20. H. Inoue, N. Miwa and N. Inakazu: *Acta Mater.*, 1996, **44**, 4825–4834.
21. L. Zhao, P. F. Willemse, J. H. Mulder, J. Beyer and W. Wei: *Scr. Mater.*, 1998, **39**, 1317–1323.
22. S. Eucken and P. Donner and E. Hornbogen: *Mater. Sci. Eng.*, 1988, **98**, 469–474.
23. S.S. Leu, Y.C. Chen and R. D. Jean: *J. Mater. Sci.*, 1992, **27**, 2792–2798.
24. S. Miyazaki, V. H. No, K. Kitamura, A. Khantachawana and H. Hosoda: *Int. J. Plast.*, 2000, **16**, 1135–1154.
25. Y. Sutou, T. Omori, A. Furukawa, Y. Takahashi, R. Kainuma, K. Yamauchi, S. Yamashita and K. Ishida: *J. Biomed., Mater. Res. Part B: Appl Biomater.* , 2004, **69B**, 64–68.
26. Y. Suzuki: in 'Shape memory materials', (ed. K. Otsuka and C. M. Wayman), 133–148; 1998, Cambridge, Cambridge Univesity Press.
27. J. Van Humbeeck and R. Stalmans: in 'Shape memory materials', (ed. K. Otsuka and C. M. Wayman), 149–177; 1998, Cambridge, Cambridge Univesity Press.
28. J. Van Humbeeck and L. Delaey: in 'The martensitic transformation in science and technology', (ed. E. Hornbogen and N. Jost), 15–25; 1989, Oberursel, DGM Informationsgesellschaft.
29. P. Tautzenberger: in 'The martensitic transformation in science and technology', (ed. E. Hornbogen and N. Jost), 213–218; 1989, Oberursel, DGM, Informationsgesellschaft.